Materials Science in Semiconductor Processing 161 (2023) 107472

Contents lists available at ScienceDirect

Materials Science in Semiconductor Processing

journal homepage: www.elsevier.com/locate/mssp

The effect of annealing treatment on the structural and optical properties of nanostructured Cu_xO films obtained by 3D printing

Vladyslav Yu. Yevdokymenko [a,*], O. Dobrozhan [a], R. Pshenychnyi [a], A. Opanasyuk [a], Yu. Gnatenko [b], A. Bukivskii [b], P. Bukivskij [b], R. Gamernyk [c], O. Klymov [d], V. Muñoz-Sanjosé [d], P. Ibañez-Romero [e], Z. Gacevic [e]

[a] Sumy State University, Rimsky-Korsakov str., 2, Sumy, UA-40007, Ukraine
[b] Institute of Physics of NASU, 46 Nauky Pr., 03028, Kyiv, Ukraine
[c] Lviv National University, 8 Kyrylo and Mefodiy Str., 29005, Lviv, Ukraine
[d] Universitat de València, C/Dr. Moliner 50, 46100, Burjassot, Spain
[e] ISOM, Universidad Politécnica de Madrid, 28040, Madrid, Spain

ARTICLE INFO

Keywords:
Cu_xO films
3D printing
Thermal annealing
Structure
Substructure
Chemical analysis
Optical characteristics

ABSTRACT

This work studies the effect of post-growth annealing on the structural and optical properties of copper oxide films. Thin films were obtained by 3D printing on glass substrates using ink based on a suspension of CuO nanoparticles. To optimize their structural characteristics and optical quality, the samples were subjected to thermal annealing for 30 min in an argon environment at different temperatures from 250 °C to 500 °C. The obtained samples were studied by scanning electron microscopy, X-ray diffraction, energy dispersive X-Ray, Raman, optical and photoelectric spectroscopy. Based on the obtained results, the main structural and substructural characteristics of the films were established, such as lattice parameters, unit cell volume, texture, sizes of coherent scattering regions, and the level of microdeformation, as well as their dependence on the annealing temperature. In addition, the nature of optical absorption, band gap energies for various types of electronic transitions, and the optical quality of the studied nanostructured copper oxide films were determined. It was shown that CuO films annealed at 350 °C have the best crystalline and optical quality. It was established that at an annealing temperature above 400 °C, a phase transition from the tenorite phase to the cuprite phase is observed. At the same time, a change in the films' substructural characteristics is already observed at T_a = 400 °C. Optimal thermal annealing conditions of Cu_xO films for effective control of their phase composition have been established.

1. Introduction

Among oxide semiconductors, copper oxide is of particular interest due to its unique electrical and photovoltaic properties, widespread availability, and low cost of components [1]. Copper, being multivalent, forms several oxides, among which CuO and Cu_2O are well-known *p*-type semiconductor materials [2]. Depending on the phase and growth method, their measured band gap is (1.3–2.1) eV for CuO and (2.1–2.6) eV for Cu_2O. The *p*-type conductivity in these oxides arises from negatively charged Cu vacancies [3]. It should be noted that the optical band gap of CuO corresponds to the Shockley-Queisser optimum for the efficiency of solar cells [4]. At the same time, copper dioxide belongs to a small group of known wide-gap compounds (NiO, Mo_xO_y, Cu_2O) with hole-type conductivity. It should be noted that Cu_2O oxide is characterized by a small effective mass of charge carriers and, accordingly, relatively high mobility, which is equal to 100 $cm^2V^{-1}s^{-1}$ or higher [5].

Cu_xO films are widely used in various electronic devices, such as thin film transistors, photoconverters, smart windows, IR detectors, gas detectors, optical filters, etc. [6]. In addition to traditional vacuum methods such as pulsed laser deposition, CVD, magnetron sputtering, etc. [7], copper oxide films have recently been deposited using low-cost non-vacuum methods, including spray pyrolysis, spin coating, printing, etc. [8].

The research on developing electronic devices and their elements using different printing techniques is actively developed [9]. 2D and 3D

* Corresponding author.
E-mail address: v.yevdokymenko@ekt.sumdu.edu.ua (V.Yu. Yevdokymenko).

https://doi.org/10.1016/j.mssp.2023.107472
Received 16 January 2023; Received in revised form 17 March 2023; Accepted 19 March 2023
Available online 1 April 2023

printing methods, which belong to the category of chemical methods, are an economical, available, flexible, and waste-free technology that significantly simplifies the procedure for production such devices and reduces their cost [10]. For 2D printing, conventional inkjet printers can be used. The ink is replaced by nanoinks containing a suspension of nanoparticles (NPs) of metals or semiconductors placed in an environmentally safe organic or aqueous medium [11]. The 3D printers allow us to develop three-dimensional elements of electronic devices of various shapes on different substrates, including human skin [12].

Usually, films obtained by chemical methods, including printing, subsequently require thermal annealing to remove chemical impurities that are part of the precursors used to synthesize NPs and inks and improve their structural characteristics [13,14]. It is known that different annealing conditions cause the formation of a mixed phase of copper oxide with other physical properties. Recent studies show that annealing of CuO in a vacuum (with conversion to Cu_2O at 500°C) improves the optical (transmission coefficient) and electrical (mobility of charge carriers) characteristics of thin films [15]. Thus, the analysis of literature data shows, by changing the annealing temperature and time, it is possible to improve the characteristics and effectively control the composition of copper oxide films. It opens up the possibility of creating, for example, isotypic *p*-Cu_2O/*p*-CuO heterojunctions suitable for use in flexible electronics or with a versatile technology to obtain films of Cu_2O for use in flexible high-performance electronics [16].

At the same time, obtaining chemically deposited Cu_xO films on transparent substrates (for example, glass) with controlled composition, high optical transparency, and hole mobility (as required when using them as active layers of electronic devices) is still an issue. It should be noted that the effect of post-growth annealing on such films' characteristics is an open subject that need more studies in order to deep on it.

The purpose of this work is to study the influence of temperature annealing (T_a = (300–500) °C) in an argon environment on the structural and optical characteristics of films obtained by 3D printing using inks based on a suspension of CuO nanoparticles to obtain single-phase oxide or dioxide copper films with controlled characteristics.

2. Materials and methods

The polyol-based synthesis carried out the synthesis of CuO NPs in the environment of distilled water. Salt $Cu(CH_3COO)_2{\cdot}H_2O$ weighing 1.2 g was dissolved in 100 ml of distilled water and 4.5 g of PVP (polyvinylpyrrolidone) when heated in a 250 ml three-necked flask. A precipitant solution was prepared separately in a beaker by dissolving 0.72 g of sodium hydroxide in 20 ml of distilled water. Then the obtained hydroxide solution was slowly added to the copper acetate solution. After that, the resulting mixture was heated to a temperature of 70 °C and kept for 60 min without overheating, with intensive mixing. The resulting product was separated from the solution by centrifugation for 10 min at 5000 rpm followed by triple washing with distilled water. Then, the resulting precipitate was diluted with distilled water until 4 ml were obtained and, finally, 1 ml of acetone was added. As a result, nanoinks based on copper oxide NPs were obtained.

Then nanostructured CuO films have been 3D printed onto a cover glass substrate with dimensions of 5 cm × 2 cm × 125 μm, by using the previously synthesized nanoink. To clean the substrate surface, the cover glass was placed in a beaker with isopropyl alcohol and sonicated for 10 min. A layer of nanoink was deposited to the dried substrates and dried in an oven for 5 min. Finally, the resulting films were annealed in an argon atmosphere at the following temperatures: 250 °C, 300 °C, 350 °C, 400 °C, 450 °C and 500 °C for 30 min. Thereafter, the samples were cooled up to room temperature naturally to prevent thermal stress cracking of the films. For comparison of samples, one sample was not annealed.

X-ray diffractometer DRON 4–07 was used to determine the structural properties of the deposited films. The analysis was carried out in Ni-filtered K_α-radiation of a copper anode. Diffractograms were recorded in continuous recording mode (speed - 16°/min, step 0.1°) in the range of 2θ angles from 20° to 80°, where 2θ is the Bragg angle. The obtained results were processed using the DifWin program. Bragg-Brentano X-ray configuration was used. The obtained diffractograms were normalized to the intensity of the (111) peak of the monoclinic phase of the compound. The phase analysis was carried out by comparing the diffraction angles from the studied samples and the diffraction angles according to JCPDS data (CuO - No. 00-048-1548, Cu_2O No. 00-005-0667 [17,18]).

The lattice constants *a, b*, and *c* of the CuO monoclinic phase were calculated using the UnitCell software, which makes it possible to calculate them from the position of all diffraction lines from the material [19].

X-ray diffraction method was also used to determine the average size of the coherent scattering regions (CSR) *L* and the level of microdeformation ε in the copper oxide films by the full width at half maximum (FWHM) and width (σ) of the diffraction lines, by using the equations [20,21]:

$$L = \frac{0.94 \bullet \lambda}{\sigma \bullet \cos\theta} \tag{1}$$

$$\varepsilon = \frac{\sigma \bullet \cos\theta}{4} \tag{2}$$

Calculations were performed based on the FWHM of reflections from crystallographic planes (20-2), (202) and (11-3) of the CuO phase, and (111), (200) and (220) of the Cu_2O phase. The reflections from copper oxide were chosen because they do not overlap with other reflections, which would complicate the interpretation of the results.

The morphology and chemical composition of copper oxide films were studied using an SEO−SEM Inspect S50–B scanning electron microscope equipped with an AZtecOne energy-dispersive spectrometer with an X-MaxN20 detector (manufactured by Oxford Instruments plc).

Raman spectra from the films were studied in the frequency range of 100–700 cm^{-1} using a Renishaw InVia 90V727 spectrometer at room temperature. Lasers with emission wavelengths of λ = 532 nm and λ = 785 nm were used as excitation radiation sources. The spectrum of each sample was measured 20 times with a time delay of 5 s. The measuring device calibration took place according to the position of the mode of oscillations of 520 cm^{-1} from a silicon crystal. Decomposition of the experimental spectra into components was carried out by representing individual peaks with a Gaussian function, which made it possible to accurately determine their position according to the frequency and FWHM of the peaks. In more detail, methods of researching oxide films are given in works [22–24].

The optical characteristics of the films were measured using a Jasco V-650 spectrophotometer in the wavelength range λ = (200–900) nm at room temperature. The spectral dependences of the optical transmittance $T(\lambda)$ and reflectance $R(\lambda)$ of thin films and their absorption were determined. The absorption spectra of the films needed to calculate E_g were found from these spectra using the equation [25,26]:

$$\alpha_l = \frac{1}{d}\ln\left(\frac{(1-R)^2}{2T} + \sqrt{\frac{(1-R)^4}{4T^2} + R^2}\right) \tag{3}$$

To determine the optical band gap E_g of materials from their absorption spectra, we used the following relationship [25,26]:

$$\alpha_l h\nu = A_0\left(h\nu - E_g\right)^n \tag{4}$$

where A_0 is a constant that depends on the effective mass of charge carriers;

$h\nu$ is the photon energy; *n* is an exponent that depends on the mechanism of photon absorption b\y the semiconductor. In the case of direct and indirect allowed band-to-band transitions, the value *n* is equal to 1/2 and 2, respectively.

It follows from this that the extrapolation of the linear section of the

graphs $(\alpha h\nu)^2 - h\nu$, $(\alpha h\nu)^{1/2} - h\nu$ on the energy axis makes it possible to determine the band gap for direct and indirect band-to-band transitions, correspondingly. In the case of direct forbidden band-band transitions it is necessary to use linearizing coordinates $(\alpha h\nu)^{2/3} - h\nu$ to determine the band gap [25–27]. Additionally, the value E_g was also determined by the absorption coefficient first derivative method [28].

3. Results and discussions

3.1. Structural and microstructural properties of Cu_xO films

Fig. 1 shows electron microscopy images of nanoparticles (a) used to create the ink and the surface of CuO films annealed at a temperature of 300 °C (b). The energy dispersive X-ray (EDX) spectrum of the annealed films can be seen on the inset of the SEM images, which ascertain the presence of copper and oxygen. As a result of research, it was established that both, particles and films, were nanostructured and contained copper and oxygen atoms. As shown in Fig. 1, nanoparticles are needle-like (narrow, long, and pointed). Their average length and width correspond to $D_1 = 117$ nm and $D_2 = 23$ nm, respectively.

The results of X-ray diffraction (XRD) analysis of annealed CuO films are shown in Fig. 2.

It was established that the diffractograms or samples annealed at temperatures T_a in the range (250–400) °C contain reflections from crystallographic planes (11-1), (111), (20-2), (202), (11-3), (31-1), (113) and (004), which correspond to the single-phase monoclinic structure of CuO (JCPDS No. 48–1548). Reflections from the (11-1) and (111) planes are dominant in the diffractograms. As the analysis shows, with an increase in the annealing temperature from 400°C to T_a in the range of (450–500) °C, the diffractograms change their appearance. Reflections from the following planes: (110), (111), (200), (220) and (311) correspond to the cubic phase of Cu_2O (JCPDS No. 05–0667). This indicates that the argon annealing process can effectively convert CuO to Cu_2O when the annealing temperature is increased to 450 °C and above. Similar behavior was observed by the authors of [15].

when the annealing temperature in a vacuum was increased to $2\bullet10^{-6}$ Torr for 2 h from 500 °C to 600 °C for CuO films obtained by the spin-coating method on SiO_2/Si substrates.

The authors of [29] found that the process of formation of crystals of the Cu_2O phase in the CuO matrix for films deposited by cathode sputtering upon annealing with an electron beam in a vacuum begins already at 450 °C. At the same time, the growth kinetics of the new phase is determined by the diffusion of oxygen along the grain boundaries of the original phase. The work [30] shows the phase diagram of the CuO→Cu_2O transition, which evidences that this temperature depends on the oxygen pressure during annealing and increases with its increases. At low oxygen pressures, this temperature is equal to 450°C, which corresponds to the data obtained in this work. However, it was

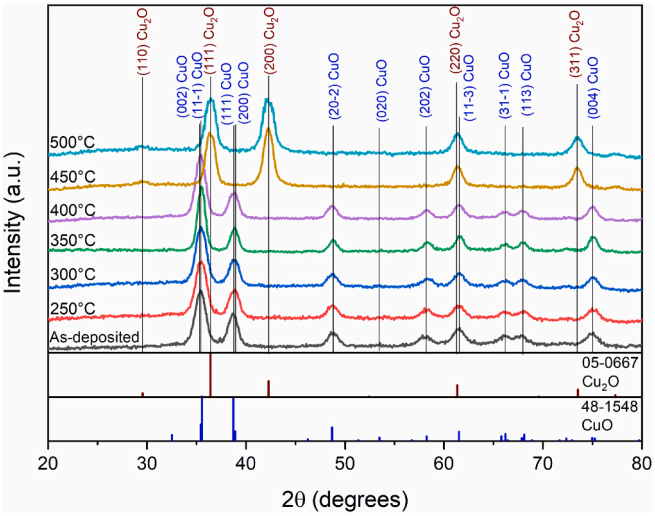

Fig. 2. Diffractograms of copper oxide films on a glass substrate, annealed in argon at different temperatures.

shown by RBS (Rutherford backscattering spectrometry) and X-ray diffraction in Ref. [30] studies, that the transition from one phase to another begins to occur even at an annealing temperature of 350 °C, and the coexistence of two phases is still observed at an annealing time of 12 h in vacuum. At the same time, individual grains of Cu_2O appear in the finely dispersed CuO matrix, and then their sizes grow linearly with the annealing time. Thus, the beginning of the transition from one oxide phase to another begins already at annealing temperatures $T_a = 350$ °C.

According to Refs. [15,30], the phase transition process from CuO to Cu_2O can be described as a desorption of oxygen from the compound into vacuum. The change in the phase composition of the films is caused by the migration of the phase boundaries between the oxides, which is due to the diffusion of oxygen in the reaction $4CuO \rightarrow 2Cu_2O + O_2$ along the moving phase boundaries. High annealing temperature provides high kinetic energy and increases the mobility of atoms. As a result, a small increase in the annealing temperature (about 50 °C) becomes effective for the transformation of the monoclinic phase into the cubic one. The authors [15] did not observe peaks from the pure copper phase in the diffractograms, which indicates that the reduction of Cu^{1+} ions to Cu^0 during annealing did not occur.

Calculations by the method of inverted pole figures allowed us to detect the [002] axial growth texture in the CuO films (Fig. 3a), while the [111] texture is observed in the Cu_2O films (Fig. 3b). The dependence of the orientation factor f on the annealing temperature T_a shown in the inset of Fig. 3, indicates the effect of this temperature on the texture quality of the samples. As can be seen from Fig. 3, the texture of

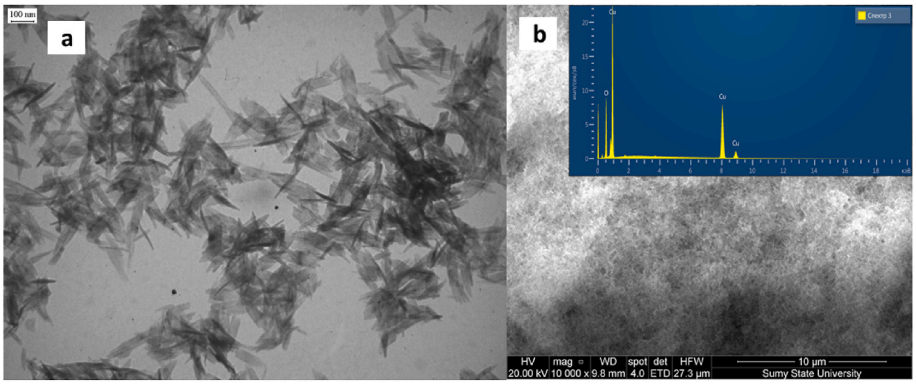

Fig. 1. (a) Surface of nanoparticles and (b) the surface of CuO films annealed at a temperature of $T_a = 300$ (°C). Inset: results of the chemical analysis of this film using EDX method.

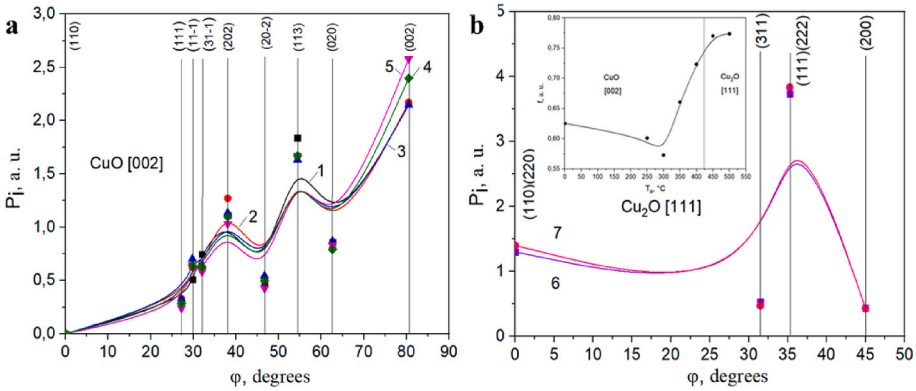

Fig. 3. Dependence of the pole density P_i from the angle φ between the texture axis and the normal to the reflecting plane for CuO (a) and Cu_2O (b) films. T_a (°C): as-deposited sample (1), 250 (2), 300 (3), 350 (4), 400 (5), 450 (6), 500 (7). Dependence of the orientation factor f from the annealing temperature T_a of samples (on the inset).

the annealed films slightly deteriorates compared to the as-deposited one when the T_a temperature is increased to 300 °C (Inset in Fig. 3). At higher temperatures, the texture quality of the films rapidly improves, which is obviously associated with the beginning of material recrystallization processes and the beginning of the formation of Cu_2O phase grains. At the same time, the process of transforming the monoclinic phase into a cubic phase leads to a change in the texture axis of the samples from the [002] texture to the [111] texture.

A change in the orientation of the texture axis [022] of CuO films obtained by the spin-coating method on SiO_2/Si substrates and subsequently annealed in a vacuum at a temperature of 400 °C to [002] when this temperature was raised to 500 °C was observed by the authors [15]. At higher temperatures (T_a = 600 °C), it was established that the CuO phase transitioned into Cu_2O, which at a temperature of T_a = 700 °C had a texture [111]. At the same time, the growth of the cubic Cu_2O phase occurred through the growth of the (111) crystallographic plane with the lowest surface energy. We also observed a similar texture in copper dioxide.

However, it should be noted that the authors [15] determined the direction of the sample texture by the presence of the most intense line on the diffractograms.

To evaluate the effect of annealing in argon on the crystal lattice of copper oxide films, its lattice parameters (a, b, c, β) and the volume of the unit cell (V), the size of the CSR (L) and the level of microdeformation (ε) in the samples were calculated. The obtained results are shown in Table 1.

The lattice parameters (a, b, c, β) of the films annealed at temperatures $T_a \leq 400$ °C, calculated using the UnitCell program, turned out to be sufficiently close to the reference values of CuO (JCPDS No. 00–48–1548) with the tenorite phase. It has been established that at the annealing temperature of T_a = (250–300) °C the values of these constants increase, but with further increase of T_a = 350°C, a sharp decrease of these values is observed. This indicates the beginning of the structural rearrangement of the crystal lattice of the material at these temperatures. It is worth to note, that at T_a = 300°C, the angle of the unit cell of the compound becomes the closest in value to the tabular one. It should be noted that at temperature.

T_a = 350°C we observed the beginning of improvement in the quality of the texture of the material. With a further increase in the temperature T_a above 350 °C, parameters a, b, c begins to grow again. In a similar way, the volume of the unit cell of the oxide behaves when the annealing temperature changes.

After increasing the annealing temperature to (450–500) °C, the values of the lattice parameters of the material and the unit cell volume (a, V) change significantly and become close (a = (0.42724–0.42741) nm, V = (77.99–78.08) × 10^{-3} nm^3) to the reference data Cu_2O (card No. 00–05–0667, a = 0.42696 nm, V = 77.83 × 10^{-3} nm^3) with a cuprite phase. A further increase in the annealing temperature at the same time leads to an increase in these parameters.

As indicated above, the substructural parameters of CuO films in the directions [20-2], [202] and [11-3] of the crystal lattice of the monoclinic phase were calculated by reflections from the crystallographic planes (20-2), (202) and (11-3). After changing the structure of the films to the cubic Cu_2O phase with an increase in the annealing temperature, the parameters of their substructure were calculated in the [111], [200] and [220] directions of the crystal lattice (by reflections from the (111), (200) and (220) planes). Table 1 shows the results of the CSR values and the level of microdeformation of the films immediately after deposition and after the annealing process.

As can be seen from Table 1, the studied films contained regions of

Table 1
Structural and substructural (using the UnitCell program) characteristics of films, corresponding to different annealing temperatures in an argon atmosphere.

Sample, T_a (°C)	A (nm)	B (nm)	C (nm)	β (°)	V_{CuO} (10^3 nm^3)	L (nm)			ε (×10^3)		
						(20-2)	(202)	(11-3)	(20-2)	(202)	(11-3)
CuO											
As-deposited	0.47079	0.34216	0.51283	99.25	81.53	7.5	6.4	6.2	4.8	5.6	5.8
250	0.47399	0.34233	0.51329	99.84	82.06	6.8	7.2	6.6	5.3	5.0	5.5
300	0.46866	0.34279	0.51276	99.54	81.23	7.2	6.6	7.5	5.1	5.5	4.8
350	0.46872	0.34117	0.51340	99.70	80.92	10.4	8.4	9.5	3.5	4.3	3.8
400	0.46990	0.34212	0.51354	99.69	81.37	7.1	7.2	7.1	5.1	5.0	5.1
JCPDS 48-1548	0.46880	0.34230	0.51320	99.51	81.22						
Cu_2O											
						(111)	(200)	(220)	(111)	(200)	(220)
450	0.42724	–	–		77.99	7.4	7.5	8.1	4.9	4.8	4.4
500	0.42741	–	–		78.08	7.4	7.5	8.2	5.6	5.6	4.4
JCPDS 05-0667	0.42696	–	–		77.83						

CSR that did not exceed $L = (6.2–7.5)$ nm in size. Up to the annealing temperature of 300 °C, this size remains practically unchanged, but when T_a is increased, it begins to grow significantly in all crystallographic directions, reaching $L = (8.4–10.4)$ nm. At the same time, the increase in size in different crystallographic directions occurs unevenly, L increases the most in the (20-2) direction, reaching 10.4 nm. At the temperature $T_a = 400$°C, there is a sharp decrease in the middle size of the CSR to (7.1–7.2) nm, which indicates the beginning of the process of formation of a new phase in the films. However, this is not yet detected by X-ray diffraction, as new peaks on the spectra.

The studied thin films were characterized by a fairly low level of microdeformation $\varepsilon = (4.8–5.8) \cdot 10^{-3}$, which slightly decreases up to the annealing temperature of 300°C. An increase of this temperature to 350°C leads to a sharp decrease in the level of microdeformation to $(3.5–4.3) \cdot 10^{-3}$. The situation changes dramatically at $T_a = 400$°C, when the level of microdeformation increases to $\varepsilon = (5.0–5.1) \cdot 10^{-3}$.

At an annealing temperature of 450 °C, as shown by X ray diffractometry, the crystallographic phase in the material changes from CuO to Cu_2O. At the same time, there is a slight increase in the size of the CSR in the films up to (7.4–8.1) nm, while microdeformation decrease slightly. A further increase in the annealing temperature leads to an increase in the size of the CSR, first of all, in the [220] direction, while in other directions this size even decreases somewhat. That is, the growth of substructural elements is selective, which determines the appearance of the growth texture in the films. This process is accompanied by an increase in the level of microdeformation, primarily in the [111] and [200] directions.

The results of determining the chemical composition of annealed copper oxide films are shown in Fig. 4. It was established that the initial films contained 54.34 at. % oxygen and 45.66 at. % copper, that is, they were enriched with oxygen compared to the stoichiometric composition of the material ($\gamma = C_{Cu}/C_O = 0.84$).

The annealing of thin films leads to a rapid decrease in oxygen concentration and an increase in copper concentration. At $T_a = 300$ °C, they contained more copper (51.14 at. %) than oxygen (48.86 at. %), and the ratio of these concentrations was $\gamma = 1.05$. These films were the closest in composition to the stoichiometric material. A further increase in the annealing temperature leads to a slight increase in the concentration of copper in the films ($C_{Cu} = 52.53$ at. %, $C_O = 47.47$ at. %, $\gamma = 1.11$ at $T_a = 400$ °C).

The situation fundamentally changed at the annealing temperature $T_a > 400$ °C. Such films were significantly copper-enriched ($C_{Cu} = (62.52–63.22)$ at. %), which confirms the X-ray analysis data on the CuO→Cu_2O phase transition. At the same time, an increase in the annealing temperature leads to an improvement in the stoichiometry of the films ($\gamma = 1.72$ at $T_a = 500$ °C). However, such films were depleted of oxygen relative to the stoichiometric composition of the material, which obviously indicates that they contain, in addition to Cu_2O, a small amount of the CuO phase. The chemical composition of the films annealed at a temperature of $T_a > 450$ °C correlates well with the data of the work [26].

3.2. Raman scattering of Cu_xO films

Raman spectroscopy is a powerful method for studying the structural characteristics of films and identifying different oxide phases due to changes in the polarization of their chemical bonds [31]. Unlike diffractograms, different copper oxides show significantly different Raman spectra since the vibrational properties of these materials depend on their crystal symmetry [32]. That is why this method was used to study the effect of annealing on the structural characteristics of the samples.

The study of the Raman spectra of the films was carried out at room temperature in the frequency range (100–700) cm^{-1}. The corresponding dependencies are presented in Fig. 5. It is known that the CuO compound belongs to the C_{2h}^6 space group with two molecules in the primitive cell.

The optical phonon modes of this oxide relative to the center of the Brillouin zone are given by the expression $\Gamma_{RA} = 4A_u + 5B_u + A_g + 2B_g$, where Γ is the degree of freedom of oscillations, A_u and B_u correspond to infrared modes; A_g and B_g are Raman modes. Thus, we have six active infrared modes ($3A_u + 3B_u$), three of which are acoustic ($A_u + 2B_u$ modes), and three are Raman ($A_g + 2B_g$ modes) [33]. As can be seen from Fig. 5, the spectrum of the as-deposited sample has an intense peak at 298 cm-1 and weak peaks at 347 cm^{-1} and 620 cm^{-1}, which correspond to phonon modes A_{1g}, B_{1g}, and B_{2g} of the crystal structure of monoclinic CuO, respectively. These frequencies correlate well with

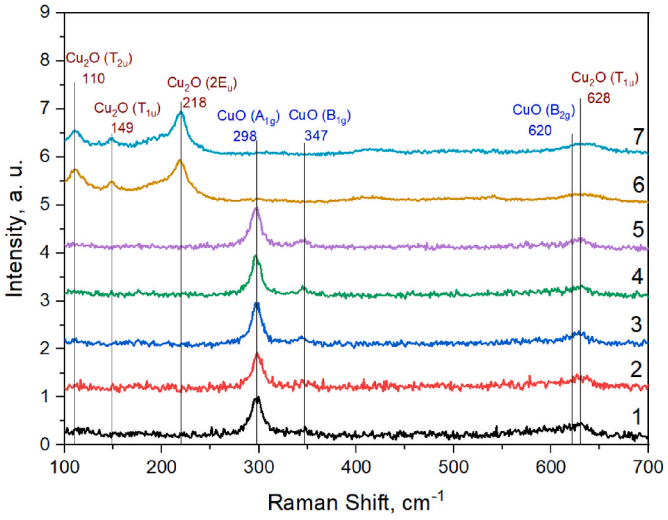

Fig. 5. Raman spectra of as-deposited (1) and annealed copper oxide films at temperatures T_a (°C): 250 (2), 300 (3), 350 (4), 400 (5), 450 (6), 500 (7).

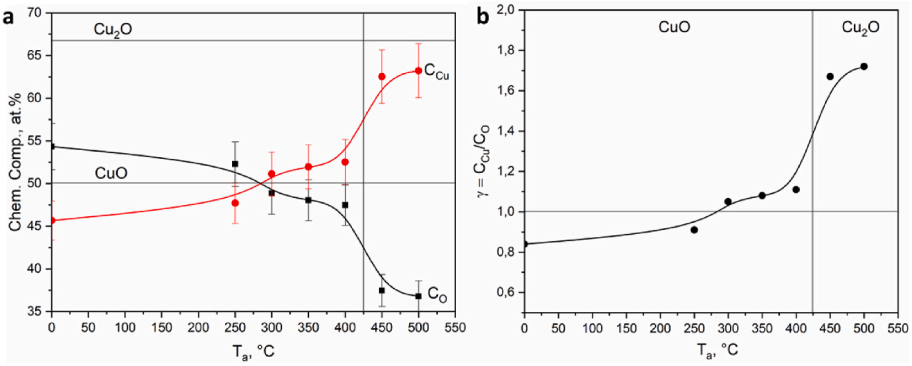

Fig. 4. Dependence of the chemical composition of Cu_xO films on the annealing temperature: atomic concentrations of C_{Cu}, C_O (a) and the C_{Cu}/C_O ratio (b).

those given in the literature. The authors [34–39] observed peaks with frequencies of (296–298), (346–350), (621–636) cm^{-1} belonging to copper oxide (see Table 2).

During the annealing of the films to a temperature of $T_a \leq 400°C$, the appearance of the Raman spectra did not change significantly. It was established that the most intense peak of the A_{1g} phonon mode monotonically decreases its FWHM compared to the as-deposited film (σ = 16.6 cm^{-1}) up to the temperature $T_a = 350°C$ ($\sigma = 13.5$ cm^{-1}), and then the FWHM slightly increases (σ = 15.0 cm^{-1}). At the same time, annealing leads to a shift in the position of this peak relative to the initial position (298 cm^{-1}), first in the direction of increasing frequency (299 cm^{-1}) and with further increase of this temperature in the direction of decreasing frequencies (297 cm^{-1}). It is known that the intensity of Raman peaks and their FWHM depend on the grain size and the quality of the film structure. Therefore, with an increase in the annealing temperature, the structural quality of the films improved up to $T_a = 350°C$ and then slightly deteriorated, which indicates the beginning of the processes of restructuring the crystal lattice. The frequency shift of the peaks for different samples indicates a change in the level of microstress in the material, which corresponds to the results of X-ray structural studies [6].

When the annealing temperature is increased to 450°C, peaks with frequencies (297–299) cm^{-1}, (344–347) cm^{-1}, and (620–628) cm^{-1} in the Raman spectra disappear, and new ones at other frequencies are formed instead. According to the theoretical analysis, the Raman spectrum of an ideal Cu_2O crystal should contain one phonon peak corresponding to the threefold-degenerate T_{2g} symmetry (the threefold-degenerate T_{2g} mode). However, the typical copper oxide Raman spectrum is much richer. It contains several signals attributed to various single-phonon scattering processes and the background associated with two-phonon scattering. This is because vibrational modes, which were forbidden for an ideal crystal, can become Raman modes due to the symmetry reduction caused by the presence of a large number of point defects [45].

We identified four Raman active phonon modes. Their frequencies correspond to (110–111) cm^{-1}, (149–150) cm^{-1}, (216–218) cm^{-1}, and (628–633) cm^{-1}. The most intense peak at the frequency (216–218) cm^{-1} is characteristic of the Cu_2O phase [40]. The high intensity of the peak indicates the film's highly ordered crystalline structure. This is one of the forbidden Raman modes of the Cu_2O phase, which becomes active due to violation of the selection rules. It arises due to the allowed Raman scattering of the second-order $2\Gamma_{12}^{-}$ mode of Cu_2O. Along with the intense peak at the frequency (216–218) cm^{-1}, peaks at (110–111) cm^{-1}, (149–150) cm^{-1} and (628–633) cm^{-1} reflect the existence of copper material in the volume with the oxidation state of Cu^+ [46]. The peak at (110–111) cm^{-1} should be inactive, but becomes active due to a large number of defects in the lattice, possibly due to oxygen vacancies, while the peak around 148 cm^{-1} is due to Raman scattering on phonons of F_{1u} symmetry. The broad peak around (628–633) cm^{-1} cannot be attributed to a certain phase since both the CuO and Cu_2O phases have spectral features at this wave number.

Table 2
Raman shift of copper oxide peaks and their interpretation.

	T_a (°C)	Raman shift (cm^{-1})					References
CuO	As-deposited	298		347		620	This study
	250	299		346		620	
	300	297		344		626	
	350	297		346		624	
	400	297		345		628	
Cu_2O	450	111		150	216	628	
	500	110		149	218	633	
CuO		298		347		591	[34]
		296		346		631	[35]
		283		330		616	[36]
		273		321		606	[37]
		296		346		631	[38]
		293		341		628	[39]
Cu_2O			218		523	623	[34]
		149	218	417		630	[40]
					525	625	[41]
		150			528	623	[42]
		155	220	410	500	630	[43]
$Cu(OH)_2$					490		[34]
		292			488		[44]
					460		[41]
		293			488		[45]

3.3. Optical absorption spectra of Cu_xO films

Fig. 6 shows the spectral dependences of the reflection coefficients $R(\lambda)$ of CuO films annealed at different temperatures. It can be seen that the as-deposited film has the lowest reflection coefficient. As the annealing temperature increases, this coefficient also increases. The increase in the reflection coefficient becomes especially noticeable at $T_a \geq 450°C$. A similar effect may be caused by a decrease in the roughness of the film surface. This confirmation is supported by the observation of interference pattern for $R(\lambda)$ spectra, which is characteristic of samples annealed at temperatures (450–500) °C. Taking into account the position of the interference maxima and minima of the spectra, the thickness of the films was precisely determined, which turned out to be equal to d = 0.443 μm.

The optical absorption of semiconductor materials is characterized by the appearance of a steep absorption edge caused by the appearance of optical transitions between the valence band and the conduction band [47]. In order to calculate the absorption coefficient α of the investigated films, the corresponding dependences of $R(\lambda)$ and $T(\lambda)$ were used.

Fig. 7a (curve 1) shows the spectral dependence of the coefficient absorption of freshly obtained nanostructured copper oxide films prepared at room temperature on a glass substrate, which indicates that the absorption edge for the films starts at about 1.40 eV. Taking into account the peculiarities of the band structure of this material [48,49], it should be assumed that the absorption in the long-wavelength spectrum region is obviously due to optical indirect allowed transitions since the value of E_g in the case of such transitions is about 1.4 eV. In the short-wavelength region of the spectrum (>1.5 eV), the steepness of the absorption edge increases.

significantly, which indicates the presence of absorption due to other, namely, direct optical transitions. As is known [49], the E_g value for direct optical transitions for CuO is 1.91 eV.

It is well known [50] that to obtain semiconductor materials,

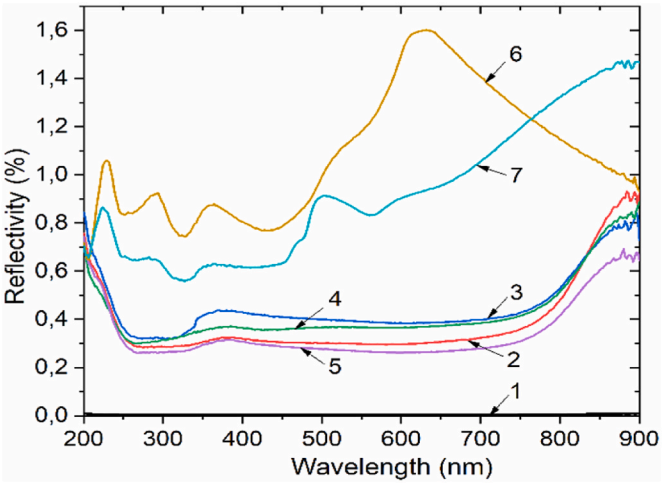

Fig. 6. Spectra of reflectance $R(\lambda)$ of as-deposited (1) and annealed copper oxide films at temperatures T_a (°C): 250 (2), 300 (3), 350 (4), 400 (5), 450 (6), 500 (7).

especially nanomaterials of high optical quality, they are annealed at high temperatures in various atmospheres. Such annealing will affect the nature and concentration of various defects in nanomaterials. And therefore, in this case, it becomes possible to optimize the chemical and technological conditions for obtaining nanomaterials with given physical properties. Thus, similar studies of the absorption edge were also carried out for copper oxide films obtained on glass substrates at different annealing temperatures (from 250°C to 500°C) and annealing time for 30 min, which also shown in Fig. 7 (curves 2–7). The obtained results indicate that when the annealing temperature increases, the absorption edge shifts to the long-wavelength region of the spectrum. It should be noted that the change in the steepness of the absorption edge may be caused by a change in the crystalline quality of the films or may reflect the different contribution of the two crystalline phases (CuO and Cu_2O) to the shape of the absorption edge.

As can be seen from Fig. 7a the absorption edge of films annealed at a temperature (250–400) °C shifts to the long-wavelength side with increasing annealing temperature in relation to the results obtained for a freshly prepared sample. In addition to the long-wavelength shift, there is also an increase in the steepness of the absorption edge. An increase in the size of the crystalline grains of the investigated films can cause the nature of the long-wavelength shift of the absorption edge. It should be noted that this result is consistent with the data presented in Table 2, where for the crystallographic direction (20-2) the size of coherent scattering, i.e., the value of L increases from 6.8 nm to 10.4 nm when the annealing temperature increases from 250°C to 350°C ed. Further increase the annealing temperature up to 400°C causes decrease in the value L to 7.4 nm, that can be caused by the formation of Cu_2O phase. Thus, we assume that the low energy shifts of the absorption edge at T_a = 400°C are also due to this case. It should be noted that nanocrystallites, as a rule, have a certain dispersion of their sizes, including those sizes for which the quantum-size effect can be manifested. Therefore, the absorption of such nanocrystallites should be caused by optical transitions involving nanoparticles with a slightly larger band gap than that of the bulk material. Thus, the shape of the absorption edge of an ensemble of nanoparticles of different sizes is determined by the superposition of their relative contributions. Therefore, with a decrease in the contribution of small-sized nanoparticles, which can occur with an increase in the average size of nanoparticles in the process of high-temperature annealing of films, the absorption edge of the films will shift to the long-wavelength side of the spectrum. Since the steepness of the absorption edge of the films increases with increasing annealing temperature from 250°C to 350°C, this also indicates an improvement in the crystalline and optical quality of the studied films in comparison with freshly prepared films. The results also show that the temperatures of 350°C are the most optimal for obtaining films with the largest average value of the size of crystalline nanograins. Thus, the films obtained at 350°C also is characterized by better optical quality. This result agrees with the data presented in Table 2, where it was shown that the level of microdeformation ε is minimum for T_a = 350°C for the different crystallographic directions.

The results of the study of the absorption edge for films annealed at a temperature of 450°C is quite different from the results obtained for other copper oxide films. Here, the absorption edge is strongly shifted to the short-wavelength side. At the same time, the value of absorption in the spectral region (<2.0 eV) is significantly reduced. There is a noticeable increase in the absorption coefficient in the longer wavelength spectral region (<1.5 eV). This, most likely, is due to the deterioration of the crystalline and optical quality of films annealed at temperatures of 450°C. One of the reasons that can cause such a deterioration of the crystal structure of copper oxide films may be the formation of a mixture of two crystalline phases, namely CuO and Cu_2O. This is also consistent with the results of structural studies presented in Table 2, which indicate the formation of a crystalline phase of Cu_2O for the films annealed at temperatures of 450°C and 500°C, which is a less stable compound than CuO. The presence of such a mixture of phases can lead to an increase in the amount of scattered light, which, accordingly, will increase the absorption background in the region of transparency of the films. On the other hand, Cu_2O nanoparticles have a larger value of the direct allowed band gap (about 2.4 eV) than the similar value for the CuO compound (1.9 eV). Thus, the presence of these phases should lead to the appearance of an additional absorption in the spectral region above 2.0 eV.

In this work, we used a simple method to determine the band gap energy based on analysis of the absorption coefficient first derivative (ACFD), taking into account the various dependencies of this value on the energy at different absorption edge [51–53]. This method can be effectively used to determine the band gap for the direct and indirect semiconductors and for ternary semiconductor alloys to evaluate their average band gap. Thus, studying the absorption spectrum of semiconductors allows us to obtain valuable information about the band structure of semiconductors.

Fig. 7b shows the ACFD values for a freshly prepared film (curve 1) and the films annealing at different temperatures (curves 2–6). The ACFD spectrum of a freshly prepared film (curve 1) contains the structure. In particular, two maximum of the spectrum is observed at 1.63 eV and 1.91 eV. In addition, a strongly tightened high-energy edge of the ACFD spectrum up to 2.6 eV was also detected. This indicates the presence of various electronic processes that lead to the formation of the absorption edge [51]. We assume that the appearance of the first maximum at 1.63 eV is obviously due to indirect allowed band-to-band transitions. It is known the energy of such transition for CuO corresponds to (1.1–1.7) eV [54]. The second maximum at 1.91 eV can be attributed to direct band-to-band transitions since its energy coincides with the value obtained theoretically in Ref. [49]. The high-energy ACFD edge in the spectral region of (2.2–2.6) eV is obviously caused

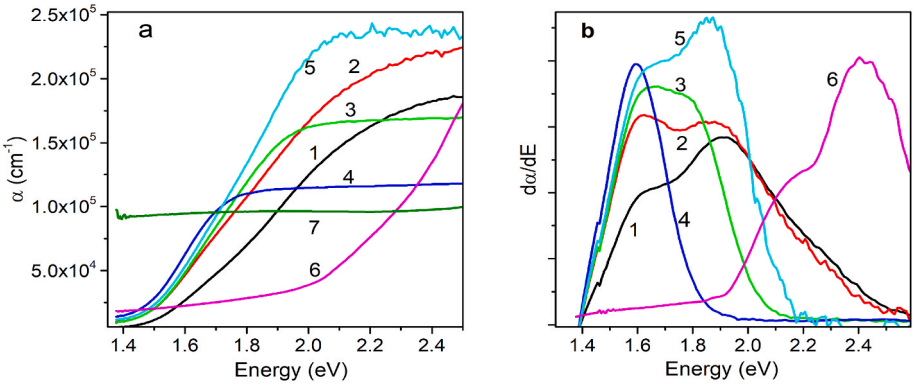

Fig. 7. Spectral dependence of the coefficient absorption (a) and the absorption coefficient first derivative (b) of the Cu_xO thin films obtained at different annealing temperatures (curves 1–7) correspond to as-deposited film and annealed at T_a (°C): 250, 300, 350, 400, 450 and 500, respectively.

by electronic processes characteristic of the Cu_2O compound. So, this result indicates a small amount of Cu_2O phase for the freshly prepared film. The temperature annealing of the films causes the following changes in the ACFD spectra. It should be noted that the ACFD spectrum obtained for the films annealed at the temperature of 250°C is similar to that for the freshly prepared films. However, in this case, the relative intensity of the first maximum of the ACFD spectrum at 1.62 eV increases. The energy position of the second maximum shifts to the low-energy region and corresponds to 1.88 eV. An increase in the annealing temperature to 300°C causes a significant decrease in the intensity of the ACFD spectrum in the spectral region (2.0–2.6) eV. The energy position of the first and second maxima correspond to 1.65 eV and 1.77 eV, accordingly. A further increase in the annealing temperature to 350°C leads to a substantial narrowing of the ACFD spectrum and the observation of only the first maximum at 1.59 eV. As can be seen from Fig. 7b, the films annealed at $T_a = 400$ °C contain two maxima at 1.66 eV and 1.86 eV and also show a prolonged high-energy edge of the ACFD spectrum. It should be noted that the second maximum is more intense than the first maximum. The ACFD spectrum of films obtained at 450°C is significantly different from other spectra. It covers the spectral region from 1.8 eV to 2.8 eV and also observes maxima at energies of 1.87 eV, 2.17 eV, and 2.41 eV.

The change in the ACFD spectrum for films annealed at different temperatures can be explained by assuming the presence of direct forbidden band-band transitions for the CuO compound at an energy of approximately 1.90 eV. The observation of these optical transitions can be due to the violation of the selection rules as a result of the presence of the Cu_2O phase for CuO films. In this case, local deformation of nanoparticles occurs. Increasing the annealing temperature leads to a decrease in the absorption intensity caused by these optical transitions as the relative contribution of the Cu_2O phase decreases. Thus, the Cu_xO films' annealing improves the investigated films' crystal and optical quality. It should be noted that the films annealed at a temperature of 350°C have the best optical quality, for which the crystalline phase of Cu_2O is practically absent. A further increase in the annealing temperature to 450 °C causes the formation of the Cu_2O phase, which becomes the determining factor. In this case, the maximum weak intensity at 1.86 eV can be associated with direct forbidden transitions that appear for the CuO phase. At the same time, other maxima at 2.17 eV and 2.41 eV correspond to direct forbidden and direct allowed transitions since these energies practically coincide with the values (2.17 eV and 2.62 eV, correspondingly) presented in Ref. [48]. It should be noted that the obtained results based on measuring the absorption spectra of the studied Cu_xO films agree very well with the results of structural studies. In particular, the obtained results of studying the optical properties of the films correlate well with the data of their X-ray structural and Raman studies, which indicate a phase transition from the CuO to Cu_2O phase just above the temperature of 400°C. In this work, we also used Tauc's method to determine the band gap energies [55]. In this case, the spectral dependence was constructed in Tauc's coordinates $(\alpha h\nu)^{1/2} - h\nu$, $(\alpha h\nu)^{2/3} - h\nu$ as well as $(\alpha h\nu)^2 - h\nu$, and the linear section of the graphs was extrapolated to the energy axis. The values of the band gap obtained ACFD and Tauc's methods are presented in Table 3.

Table 3
Values of band gap energies of Cu_xO films annealed at different temperatures for various band-band transitions.

Type of the band-band transitions/Annealing temperature.	T_a (°C)					
	As-deposited	250	300	350	400	450
Indirect allowed band gap (eV). ACFD method (CuO).	1.63	1.62	1.65	1.59	1.66	–
Direct forbidden band gap (eV). ACFD method (CuO).	1.91	1.88	1.77	–	1.66	1.87
Direct forbidden band gap (eV). ACFD method (Cu_2O).	–	–	–	–	–	2.17
Direct allowed band gap (eV). ACFD method (Cu_2O).	–	–	–	–	–	2.41
Indirect forbidden band gap (eV). Tauc's method (CuO).	1.63	1.50	1.50	1.46	1.51	–
Direct forbidden band gap (eV). Tauc's method (CuO).	1.81	1.75	1.67	1.55	1.74	–

3.4. Photoconductivity spectra of Cu_xO films

In order to obtain additional information about the band structure of copper oxide films, studies of their photoelectric properties were carried out. In this case photoconductivity spectra were measured for the investigated films. Fig. 8 shows the spectra of photoconductivity at $T =$ 300 K for the films annealed at $T_a = 400$°C (curve 1) and 450°C (curve 2). The photoconductivity spectrum (curve 1) exhibits a broad maximum at 500 nm (2.48 eV), as well as a feature in the form of an inflection at 618 nm (2.01 eV), which is marked by an arrow. The energy of the photoconductivity maximum is quite close to the value of the direct band gap of the Cu_2O compound ($E_g = 2.41$ eV). Therefore, it can be assumed that this photoconductivity maximum is associated with direct band-to-band transitions of the crystalline phase of Cu_2O. At the same time, the appearance of the peculiarity of the photoconductivity spectrum at 618 nm (2.01 eV) may be associated with the direct band-to-band transitions of CuO phase since the energy of such transitions correspond to 1.91 eV. Photoconductivity spectrum obtained for a film annealed at.

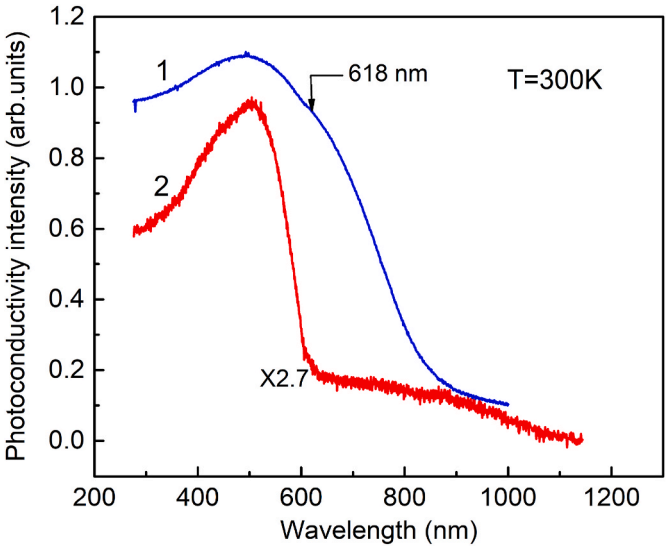

Fig. 8. Photoconductivity spectra of films annealed at 400 (°C) (curve 1) and 450 (°C) (curve 2).

a temperature of 450°C (curve 2), is significantly different in shape from the photoconductivity spectrum represented by curve 1. In particular, the intensity of photoconductivity significantly decreases in the spectral region above 600 nm. According to the results of absorption measurements, photoconductivity in this spectral region can be caused by direct and indirect band-to-band transitions associated with the CuO phase. It indicates that the intensity of photoconductivity in the long-wavelength range of the spectrum (>650 nm) is much smaller in comparision with the films annealed at 400°C. Thus, this means that for the films annealed at 450°C, there is a relatively small contribution of the crystalline CuO phase compared to that for the Cu_2O phase. It should be

noted that the obtained results agree very well with the results of measurements of absorption and Raman scattering spectra, as well as data of structural studies.

4. Conclusion

This work studies the effect of post-annealing in argon environment at temperatures from 250 °C to 500 °C on the structural, microstructural, optical, and photoelectric characteristics, as well as the chemical composition of Cu_xO films deposited on glass substrates by 3D printing. It is shown that the layers annealed at (250–400) °C have a monoclinic structure. Increasing the annealing temperature to (450–500) °C induces a transition to the cubic Cu_2O phase. This phase transition is accompanied changes in the size of crystalline grains and the level of microstrains. It was established the energies of direct and indirect band-to-band transitions of the CuO and Cu_2O phases and their dependence on the annealing temperature.

We believe that copper oxide films obtained by a simple and inexpensive 3D printing method can be considered as a promising material for use in modern optoelectronics, flexible electronics, and especially in the development of efficient and environmentally friendly third-generation solar cells. Our further work involves obtaining multilayer structures based on copper oxide films for use in such devices.

CRediT authorship contribution statement

Vladyslav Yu. Yevdokymenko: Writing – original draft, Visualization, Conceptualization. **O. Dobrozhan:** Writing – review & editing, Supervision. **R. Pshenychnyi:** Investigation. **A. Opanasyuk:** Writing – original draft, Supervision, Methodology, Funding acquisition, Conceptualization. **Yu Gnatenko:** Writing – original draft, Supervision, Resources. **A. Bukivskii:** Investigation. **P. Bukivskij:** Investigation. **R. Gamernyk:** Investigation. **O. Klymov:** Writing – review & editing, Resources, Project administration. **V. Muñoz-Sanjosé:** Writing – review & editing, Supervision, Resources, Funding acquisition. **P. Ibañez-Romero:** Investigation. **Z. Gacevic:** Investigation.

Declaration of competing interest

The authors declare that they have no known competing financial interests or personal relationships that could have appeared to influence the work reported in this paper.

Data availability

No data was used for the research described in the article.

Acknowledgments

This work was supported by the Science for Peace and Security Programme for NATO [grant number G5916] and the Ministry of Education and Science of Ukraine (0122U000787). The coauthors from the Spanish institutions want to acknowledge, too, the financial support from the Generalitat Valenciana under project Prometeo/2021/066.

References

[1] K.R. Balasubramaniam, V.M. Kao, J. Ravichandran, P.B. Rossen, W. Siemons, J. W. Ager, Semiconductor thin films directly from minerals-study of structural, optical, and transport characteristics of Cu_2O thin films from malachite mineral and synthetic CuO, Thin Solid Films 520 (2012) 3914–3917, https://doi.org/10.1016/j.tsf.2012.01.041.

[2] D.S. Murali, S. Kumar, R.J. Choudhary, A.D. Wadikar, M.K. Jain, A. Subrahmanyam, Synthesis of Cu_2O from CuO thin films: optical and electrical properties, AIP Adv. 5 (2015), 047143, https://doi.org/10.1063/1.4919323.

[3] Y. Peng, Z. Zhang, T. Viet Pham, Y. Zhao, P. Wu, J. Wang, Density functional theory analysis of dopants in cupric oxide, J. Appl. Phys. 111 (2012), 103708, https://doi.org/10.1063/1.4719059.

[4] YuH.L. Ribeiro, J.S. Pereira, D.G.F. David, M.V.S. Silva, Growth, characterization, and photovoltaic application of copper oxide thin films, Thin Solid Films 757 (2022), 139381, https://doi.org/10.1016/j.tsf.2022.139381.

[5] D. Wojcieszak, A. Obstarczyk, E. Mańkowska, M. Mazur, D. Kaczmarek, K. Zakrzewska, P. Mazur, J. Domaradzki, Thermal oxidation impact on the optoelectronic and hydrogen sensing properties of *p*-type copper oxide thin films, Mater. Res. Bull. 147 (2022), 111646, https://doi.org/10.1016/j.materresbull.2021.111646.

[6] V.G. Akkili, R. Thangavel, V.M. Srivastava, Improvement of CuO thin film properties for high mobility p-channel TFT applications, in: 2021 44th Int. Spring Semin. Electron. Technol., IEEE, 2021, pp. 1–5, https://doi.org/10.1109/ISSE51996.2021.9467529.

[7] B.E. Al-Jumaili, J.M. Rzaij, A.S. Ibraheam, Nanoparticles of CuO thin films for room temperature NO_2 gas detection: annealing time effect, Mater. Today Proc. 42 (2021) 2603–2608, https://doi.org/10.1016/j.matpr.2020.12.588.

[8] S. Muthukrishnan, V. Subramaniam, T. Mahalingam, S.J. Helen, P. Sumathi, Improved properties of spray pyrolysed CuO nanocrystalline thin films, J. Mater. Sci. Mater. Electron. 28 (2017) 4211–4218, https://doi.org/10.1007/s10854-016-6043-7.

[9] N. Marjanovic, J. Hammerschmidt, J. Perelaer, S. Farnsworth, I. Rawson, M. Kus, E. Yenel, S. Tilki, U.S. Schubert, R.R. Baumann, Inkjet printing and low temperature sintering of CuO and CdS as functional electronic layers and Schottky diodes, J. Mater. Chem. 21 (2011), 13634, https://doi.org/10.1039/c1jm11237f.

[10] M.S. Rager, T. Aytug, G.M. Veith, P. Joshi, Low-thermal-budget photonic processing of highly conductive Cu interconnects based on CuO nanoinks: potential for flexible printed electronics, ACS Appl. Mater. Interfaces 8 (2016) 2441–2448, https://doi.org/10.1021/acsami.5b12156.

[11] P. Krcmar, I. Kuritka, J. Maslik, P. Urbanek, P. Bazant, M. Machovsky, P. Suly, P. Merka, Fully inkjet-printed CuO sensor on flexible polymer substrate for alcohol vapours and humidity sensing at room temperature, Sensors 19 (2019) 3068, https://doi.org/10.3390/s19143068.

[12] F. Fayyazbakhsh, M.C. Leu, A brief review on 3D bioprinted skin substitutes, Procedia Manuf. 48 (2020) 790–796, https://doi.org/10.1016/j.promfg.2020.05.115.

[13] R. Agarwal, K. Verma, N.K. Agrawal, R.K. Duchaniya, R. Singh, Synthesis, characterization, thermal conductivity and sensitivity of CuO nanofluids, Appl. Therm. Eng. 102 (2016) 1024–1036, https://doi.org/10.1016/j.applthermaleng.2016.04.051.

[14] H.Y. Jun, E.J. Lee, S.O. Ryu, Synthesis and characterization of copper ink and direct printing of copper patterns by inkjet printing for electronic devices, Curr. Appl. Phys. 20 (2020) 853–861, https://doi.org/10.1016/j.cap.2020.04.003.

[15] J. Yu, G. Liu, A. Liu, Y. Meng, B. Shin, F. Shan, Solution-processed p-type copper oxide thin-film transistors fabricated by using a one-step vacuum annealing technique, J. Mater. Chem. C 3 (2015) 9509–9513, https://doi.org/10.1039/C5TC02384J.

[16] M. Dhaouadi, Physical properties of copper oxide thin films prepared by sol–gel spin–coating method, Am. J. Phys. Appl. 6 (2018) 43, https://doi.org/10.11648/j.ajpa.20180602.13.

[17] H. Gleiter, Nanocrystalline solids, J. Appl. Crystallogr. 24 (1991) 79–90, https://doi.org/10.1107/S0021889890011013.

[18] H.E. Swanson, R.K. Fuyat, Standard X-Ray Diffraction Powder Patterns, N.B.S. CIR. 539, 1953, p. 2. Reference to a book: https://nvlpubs.nist.gov/nistpubs/Legacy/circ/nbscircular539v2.pdf.

[19] T.J.B. Holland, S.A.T. Redfern, UNITCELL : a nonlinear least-squares program for cell-parameter refinement and implementing regression and deletion diagnostics, J. Appl. Crystallogr. 30 (1997), https://doi.org/10.1107/S0021889896011673, 84–84.

[20] L. Attou, B. Jaber, H. Ez-Zahraouy, Effect of annealing temperature on structural, optical and photocatalytic properties of CuO nanoparticles, Mediterr. J. Chem. 7 (5) (2018) 308–316, https://doi.org/10.13171/mjc751911261230la.

[21] N. Prasad, V.M.M. Saipavitra, H. Swaminathan, P. Thangaraj, M. Ramalinga Viswanathan, K. Balasubramanian, Microstress, strain, band gap tuning and photocatalytic properties of thermally annealed and Cu-doped ZnO nanoparticles, Appl. Phys. A 122 (2016) 590, https://doi.org/10.1007/s00339-016-0121-9.

[22] O. Dobrozhan, M. Baláž, P. Baláž, S. Vorobiov, A. Opanasyuk, Morphological, structural, microstructural, chemical properties of nanostructured Cu_2ZnSnS_4 flexible thin films obtained by inkjet printing of polyol-mediated nanocrystals, J. Alloys Compd. 842 (2020), 155883, https://doi.org/10.1016/j.jallcom.2020.155883.

[23] D. Kurbatov, A. Opanasyuk, S. Duvanov, A. Balogh, H. Khlyap, Growth kinetics and stoichiometry of ZnS films, Solid State Sci. 13 (2011) 1068–1071, https://doi.org/10.1016/j.solidstatesciences.2011.01.017.

[24] O. Dobrozhan, O. Diachenko, M. Kolesnyk, A. Stepanenko, S. Vorobiov, P. Baláž, S. Plotnikov, A.S. Opanasuyk, Morphological, structural and optical properties of Mg-doped ZnO nanocrystals synthesized using polyol process, Mater. Sci. Semicond. Process. https://doi.org/10.1016/j.mssp.2019.104595.

[25] Y. Znamenshchykov, V. Kosyak, V. Kononov, I. Shpetnyi, V. Grebinaha, P. Fochuk, A. Opanasyuk, Electrical, structural and optical properties of $Cd_{1-x}Zn_xTe$ thick polycrystalline films, Vacuum 149 (2018) 270–278, https://doi.org/10.1016/j.vacuum.2018.01.010.

[26] F.A. Akgul, G. Akgul, N. Yildirim, H.E. Unalan, Influence of thermal annealing on microstructural, morphological, optical properties and surface electronic structure of copper oxide thin films, Mater. Chem. Phys. 147 (2014) 987–995, https://doi.org/10.1016/j.matchemphys.2014.06.047.

[27] D.O. Rivera, G.T. Delgado, J.M. Marín, R.C. Pérez, M.A.A. Frutis, O.Z. Ángel, Cuprous oxide thin films obtained by spray-pyrolysis technique, J. Mater. Sci.

Mater. Electron. 29 (2018) 851–857, https://doi.org/10.1007/s10854-017-7980-5.
[28] N.A. Che Lah, P. Murthy, M.N. Mohd Zubir, The physical and optical investigations of the tannic acid functionalised Cu-based oxide nanostructures, Sci. Rep. 12 (2022) 9909, https://doi.org/10.1038/s41598-022-14281-z.
[29] J. Li, S.Q. Wang, J.W. Mayer, K.N. Tu, Oxygen-diffusion-induced phase boundary migration in copper oxide thin films, Phys. Rev. B 39 (1989) 12367–12370, https://doi.org/10.1103/PhysRevB.39.12367.
[30] J. Li, G. Vizkelethy, P. Revesz, J.W. Mayer, K.N. Tu, Oxidation and reduction of copper oxide thin films, J. Appl. Phys. 69 (1991) 1020–1029, https://doi.org/10.1063/1.347417.
[31] F. Wu, S. Banerjee, H. Li, Y. Myung, P. Banerjee, Indirect phase transformation of CuO to Cu_2O on a nanowire surface, Langmuir 32 (2016) 4485–4493, https://doi.org/10.1021/acs.langmuir.6b00915.
[32] Y. Alajlani, F. Placido, A. Barlow, H.O. Chu, S. Song, S. Ur Rahman, R. De Bold, D. Gibson, Characterisation of Cu_2O, Cu_4O_3 , and CuO mixed phase thin films produced by microwave-activated reactive sputtering, Vacuum 144 (2017) 217–228, https://doi.org/10.1016/j.vacuum.2017.08.005.
[33] K. Mageshwari, R. Sathyamoorthy, Flower-shaped CuO nanostructures: synthesis, characterization and antimicrobial activity, J. Mater. Sci. Technol. 29 (2013) 909–914, https://doi.org/10.1016/j.jmst.2013.04.020.
[34] Y. Deng, A.D. Handoko, Y. Du, S. Xi, B.S. Yeo, In situ Raman spectroscopy of copper and copper oxide surfaces during electrochemical oxygen evolution reaction: identification of Cu^{III} oxides as catalytically active species, ACS Catal. 6 (2016) 2473–2481, https://doi.org/10.1021/acscatal.6b00205.
[35] L. Debbichi, M.C. Marco de Lucas, J.F. Pierson, P. Krüger, Vibrational properties of CuO and Cu_4O_3 from first-principles calculations, and Raman and infrared spectroscopy, J. Phys. Chem. C 116 (2012) 10232–10237, https://doi.org/10.1021/jp303096m.
[36] A. Maini, M.A. Shah, Sol-gel fabricated CuO thin film: characterization for device application, J. Nano- Electron. Phys. 13 (2021), https://doi.org/10.21272/jnep.13(5).05018, 05018-1-05018–5.
[37] W. Wang, Z. Liu, Y. Liu, C. Xu, C. Zheng, G. Wang, A simple wet-chemical synthesis and characterization of CuO nanorods, Appl. Phys. Mater. Sci. Process 76 (2003) 417–420, https://doi.org/10.1007/s00339-002-1514-5.
[38] R. Panda, M. Patel, J. Thomas, H.C. Joshi, Pulsed laser deposited Cu_2O/CuO films as efficient photocatalyst, Thin Solid Films 744 (2022), 139080, https://doi.org/10.1016/j.tsf.2022.139080.
[39] A. Prakash, G.V.S. Krishna, S.N. Moger, M.G. Mahesha, Spectroscopic and electrical analysis of spray deposited copper oxide thin films, Mater. Today Commun. 32 (2022), 103926, https://doi.org/10.1016/j.mtcomm.2022.103926.
[40] A. Dey, G. Chandrabose, L.A.O. Damptey, E.S. Erakulan, R. Thapa, S. Zhuk, G. K. Dalapati, S. Ramakrishna, N.S.J. Braithwaite, A. Shirzadi, S. Krishnamurthy, Cu_2O/CuO heterojunction catalysts through atmospheric pressure plasma induced defect passivation, Appl. Surf. Sci. 541 (2021), 148571, https://doi.org/10.1016/j.apsusc.2020.148571.
[41] H.Y.H. Chan, C.G. Takoudis, M.J. Weaver, Oxide film formation and oxygen adsorption on copper in aqueous media as probed by surface-enhanced Raman spectroscopy, J. Phys. Chem. B 103 (1999) 357–365, https://doi.org/10.1021/jp983787c.
[42] G. Niaura, Surface-enhanced Raman spectroscopic observation of two kinds of adsorbed OH^- ions at copper electrode, Electrochim. Acta 45 (2000) 3507–3519, https://doi.org/10.1016/S0013-4686(00)00434-5.
[43] A. Singhal, M.R. Pai, R. Rao, K.T. Pillai, I. Lieberwirth, A.K. Tyagi, Copper(I) oxide nanocrystals – one step synthesis, characterization, formation mechanism, and photocatalytic properties, Eur. J. Inorg. Chem. 2013 (2013) 2640–2651, https://doi.org/10.1002/ejic.201201382.
[44] T.H. Tran, V.T. Nguyen, Phase transition of Cu_2O to CuO nanocrystals by selective laser heating, Mater. Sci. Semicond. Process. 46 (2016) 6–9, https://doi.org/10.1016/j.mssp.2016.01.021.
[45] D. Reyter, M. Odziemkowski, D. Bélanger, L. Roué, Electrochemically activated copper electrodes, J. Electrochem. Soc. 154 (2007) K36, https://doi.org/10.1149/1.2746805.
[46] T. Sander, C.T. Reindl, M. Giar, B. Eifert, M. Heinemann, C. Heiliger, P.J. Klar, Correlation of intrinsic point defects and the Raman modes of cuprous oxide, Phys. Rev. B 90 (2014), 045203, https://doi.org/10.1103/PhysRevB.90.045203.
[47] Yu Gnatenko, P. Bukivskij, M. Furier, A. Bukivskii, A. Opanasyuk, Temperature dependence of the band gap of high optical quality CdS:Dy thin films based on exciton spectra, Mater. Res. Express 5 (2018), 125902, https://doi.org/10.1088/2053-1591/aae298.
[48] Y. Wang, S. Lany, J. Ghanbaja, Y. Fagot-Revurat, Y.P. Chen, F. Soldera, D. Horwat, F. Mücklich, J.F. Pierson, Electronic structures of Cu_2O, Cu_4O_3, and CuO: a joint experimental and theoretical study, Phys. Rev. B Condens. Matter 94 (2016), 245418, https://doi.org/10.1103/PhysRevB.94.245418.
[49] M. Heinemann, B. Eifert, C. Heiliger, Band structure and phase stability of the copper oxides Cu_2O, CuO, and Cu_4O_3, Phys. Rev. B 87 (2013), 115111, https://doi.org/10.1103/Phys Rev B.87.115111.
[50] O. Diachenko, J. Kovác Jr., O. Dobrozhan, P. Novák, J. Kovác, J. Skriniarova, A. Opanasyuk, Structural and optical properties of CuO thin films synthesized using spray pyrolysis method, Coatings 20 11 (2021) 1392, https://doi.org/10.3390/coatings11111392.
[51] W.Z. Shen, A novel approach for the evaluation of band gap energy in semiconductors, Int. J. Infrared Millimet. Waves 23 (2002) 61–69, https://doi.org/10.1023/A:1015033901163.
[52] J. Tamayo-Arriola, A. Huerta-Barbera, M. Montes Bajo, E. Munoz, V. Munoz-Sanjos, A. Hierro, Rock-salt CdZnO as a transparent conductive oxide, Appl. Phys. Lett. 113 (2018), 222101, https://doi.org/10.1063/1.5048771.
[53] B. Ullrich, G.J. Brown, H. Xi, Semiconductor band gap localization via Gaussian function, Semicond. Sci. Technol. 27 (2012), 105016, https://doi.org/10.1088/0268-1242/27/10/105016.
[54] G. Mahendra, R. Malathi, S.P. Kedhareswara, A. Lakshmi-Narayana, M. Dhananjaya, N. Guruprakash, O.M. Hussain, A. Mauger, C.M. Julien, RF sputter-deposited nanostructured CuO films for micro-supercapacitors, Appl. Nanosci. 2 (2021) 46–66, https://doi.org/10.3390/applnano2010005.
[55] G. Mamba, C. Pulgarin, J. Kiwi, M. Bensimon, S. Rtimi, Synchronic coupling of $Cu_2O(p)$/CuO(n) semiconductors leading to Norfloxacin degradation under visible light: kinetics, mechanism and film surface properties, J. Catal. 353 (2017) 133–140, https://doi.org/10.1016/j.jcat.2017.06.036.